Title
Exploring feedback-controlled versus open-circuit electrochemical lipolysis in ex vivo and in vivo porcine fat: A feasibility study

Journal
Lasers in Surgery and Medicine, 54(1)

ISSN
0196-8092

Authors
Heidari, Andrew E
Hong, Ellen M
Park, Asher
et al.

Publication Date
2022

DOI
10.1002/lsm.23466

HHS Public Access

Author manuscript

Lasers Surg Med. Author manuscript; available in PMC 2023 January 01.

Published in final edited form as:

Lasers Surg Med. 2022 January ; 54(1): 157–169. doi:10.1002/lsm.23466.

Exploring Feedback Controlled versus Open Circuit Electrochemical Lipolysis in Ex Vivo and In Vivo Porcine Fat, a Feasibility Study

Andrew E. Heidari, PhD[1,2], **Ellen M. Hong, BA**[1], **Asher Park, BS**[1], **Tiffany T. Pham, MD, MS**[1,a], **Earl Steward, BS**[3], **Lily Y. Chen, BS**[1,b], **Yueqiao Qu, PhD**[1,2], **Brandyn S. Dunn, MD**[1,4], **Soo Hong Seo, MD**[1,5], **Urja Patel**[1,2], **Katelyn Dilley**[1,2], **Amir A. Hakimi, BS**[1], **Adeela Syed, PhD**[6], **Sehwan Kim, PhD**[7], **Michael G. Hill, PhD**[8], **Joon S. You, PhD**[9], **Brian J. F. Wong, MD PhD.**[1,2,4]

[1]Beckman Laser Institute & Medical Clinic, University of California - Irvine, CA 92612, USA

[2]Department of Biomedical Engineering, University of California - Irvine, Irvine, CA 92697, USA

[3]Department of Surgery, University of California - Irvine, School of Medicine, Orange, CA 92868, USA

[4]Department of Otolaryngology - Head and Neck Surgery, University of California - Irvine, School of Medicine, Orange, CA 92868, USA

[5]Department of Dermatology, Korea University, College of Medicine, Seoul, 02841, Republic of Korea

[6]Department of Developmental and Cell Biology, University of California - Irvine, CA 92697, USA

[7]Beckman Laser Institute-Korea, Department of Biomedical Engineering, Dankook University, Cheonan-si, Chungnam 31116, Republic of Korea

[8]Department of Chemistry, Occidental College, Los Angeles, CA 90041, USA

[9]Incipian LLC, Laguna Niguel, 92677

Abstract

Objectives: Minimally invasive fat sculpting techniques are becoming more widespread with the development of office-based devices and therapies. Electrochemical Lipolysis (ECLL) is a needle-based technology that uses DC current to electrolyze tissue water creating acid and base in situ. In turn, fat is saponified and adipocyte cell membrane lysis occurs. The electrolysis of water can be accomplished using a simple open loop circuit (V-ECLL) or by incorporating a feedback control circuit using a potentiostat (P-ECLL). A potentiostat utilizes an operational amplifier with negative feedback to allow users to precisely control voltage at specific electrodes. To date, the variation between the two approaches has not been studied. The aim of this study was to assess

Corresponding Author: Brian J.F. Wong, MD PhD, Phone: 949-824-7980, Beckman Laser Institute, 1002 Health Sciences Road, Irvine, CA 92697, bjwong@uci.edu.

[a]Department of Otolaryngology-Head and Neck Surgery, University of Colorado Anschutz Medical Campus, Aurora, CO 80045, USA

[b]College of Medicine, University of Central Florida, Orlando, FL 32827, USA

Conflicts of Interest: The authors have no financial interests, activities, relationships, or affiliations with respect to this study.

current and charge transfer variation and lipolytic effect created by the two approaches in an in vivo porcine model.

Methods: Charge transfer measurements from ex vivo V-ECLL and P-ECLL treated porcine skin and fat were recorded at −1V P-ECLL, −2V P-ECLL, −3V P-ECLL and −5V V-ECLL each for 5 minutes to guide dosimetry parameters for in vivo studies. Follow up in vivo studies comprised of a sedated female Yorkshire pig treated with both V-ECLL and P-ECLL across the dorsal surface over a range of dosimetry parameters including −1.5V P-ECLL, −2.5V P-ECLL, −3.5V P-ECLL and 5V V-ECLL each treated for 5 minutes. Serial examination biopsies were performed at baseline prior to treatment, 1, 2, 7, 14, and 28 days after treatment. Tissue was examined using fluorescence microscopy and histology to compare effects of the two ECLL approaches.

Results: Both V-ECLL and P-ECLL treatments induced in vivo fat necrosis evident by adipocyte membrane lysis, adipocyte denuclearization, and an acute inflammatory response across a 28-day longitudinal study. However, −1.5V P-ECLL produced a smaller spatial necrotic effect compared to 5V V-ECLL. In addition, 5V V-ECLL produced a comparable necrotic effect to that of −2.5V and −3.5V P-ECLL.

Conclusions: V-ECLL and P-ECLL at aforementioned dosimetry parameters both achieved fat necrosis by adipocyte membrane lysis and denuclearization. The −2.5V and −3.5V P-ECLL treatments created spatially similar fat necrotic effects when compared to 5V V-ECLL treatment. Quantitatively, total charge transfer between dosimetry parameters suggests that −2.5V P-ECLL and 5V V-ECLL produce comparable electrochemical reactions. Such findings suggest that a low-voltage closed-loop potentiostat-based system is capable of inducing fat necrosis to a similar extent compared to that of a higher voltage direct current system.

Keywords

Fat sculpting; fat necrosis; fat reduction; lipolysis; electrochemistry; electrochemical lipolysis; body contouring; minimally invasive cosmetic procedures

Introduction

As of 2018, the body fat contouring market was valued over $8.2 billion with an expected increase to $16.5 billion by 2025.[1] Eighty percent of this growth is attributed to surgical fat reduction technologies such as liposuction and abdominoplasty.[2] Although popular, such invasive surgical techniques generally require some degree of sedation or anesthesia, as well as recovery time before patients are able to return to work.[3] Hence, there has been increased interest in minimally- and non-invasive office-based fat reduction techniques with lower cost base and shorter recovery time. Such technologies include radiofrequency,[4] photobiomodulation,[5] high intensity focused ultrasound (HIFU),[6] cryolipolysis,[7] and deoxycholic acid injections.[8] Although effective in reducing fat, these technologies may be expensive, require multiple treatments, or lack spatial selectivity in fat contouring. We have recently developed an electrochemical method to treat fat which builds upon previous work using electrochemical techniques to reshape cartilage.[9–25]

Electrochemical lipolysis (ECLL) relies upon the electrolysis of water to create active species that lyse cell membranes and saponify triglycerides. In ECLL, tissue is first

tumesced with saline, followed by the insertion of platinum needle electrodes into the adipose layer. Electrodes are then connected to a simple DC power supply (e.g. battery) and water is electrolyzed into acid at the anode and base at the cathode through the reactions $2H_2O \rightarrow O_2 + 4H^+ + 4e^-$ and $2H_2O + 2e^- \rightarrow H_2 + 2OH^-$, respectively. Previous studies have shown this in situ acid and base generation leads to localized tissue injury facilitating cartilage reshaping, collagen remodeling in skin, tendon lengthening in joints, and adipocyte necrosis in fat with triglyceride saponification.[9–25] It should be noted that the standard limitations of electrical devices in the DC regime apply to this electrochemical therapy,[26] limiting the patient population to which this treatment is applicable. While our group has previously demonstrated the feasibility of a simple voltage driven ECLL (V-ECLL) which uses an open loop DC circuit to lyse fat, the lack of feedback control may limit reaction rate and spatial control of this electrochemical effect. Incorporating a feedback circuit to optimize current may overcome such limitations.[15] Provided that the electrochemical reaction is not reagent limited (i.e., water loss due to consumption), a desired amount of acid and/or base product can be generated in a controlled manner.

Potentiostats provide feedback control and are the most commonly used electrochemical analytic devices.[27] Whereas V-ECLL systems consist of an anode and cathode, potentiostats engage three electrodes: a working, counter, and reference electrode connected by an operational amplifier. The potentiostat maintains a user-selected potential at the working electrode by applying a sufficient voltage at the counter electrode. The counter electrode is in electrical contact with the working electrode via the surrounding electrolyte solution, and the voltage at the counter electrode is continually adjusted to provide a constant potential at the working electrode via feedback from the reference electrode. We have termed the use of a potentiostat in electrochemical lipolysis as potential-driven feedback ECLL (P-ECLL). In this system, a specific electrical potential can be applied to an array of electrodes where discrete electrochemical reactions can be isolated (Appendix A).

Herein, we compared the effects of V-ECLL and P-ECLL in an in vivo porcine model over the course of 28 days. To estimate dosimetry parameters, the experiment was prefaced with a study of current and total charge transfer of V-ECLL and P-ECLL applied to ex vivo porcine skin and fat tissue. The determined treatment parameters were then applied in vivo, and the efficacy of each treatment was assessed using fluorescence assays, visualizing cell morphology and viability, and histology. We hypothesize that P-ECLL can improve induction of adipocyte membrane lysis, denucleation, and fat necrosis compared to V-ECLL by allowing more efficient control and optimization of current.

Materials and Methods

Ex Vivo Current Analysis

Skin and fat tissue from the submental, neck, and dorsal areas of postmortem Yorkshire pigs (obtained from a local packing house or from euthanized animals used in other Institutional Animal Care and Use Committee-approved protocols) were freshly procured, wrapped and maintained in Hanks Balanced Salt Solution (HBSS) soaked gauze, and transported in a sealed container for further processing and treatment. Large segments of intact tissue were sectioned into 1 by 1 by 2 cm samples. Each tissue sample was tumesced with the

injection of 1 and 0.5 ml of normal saline into the subcutaneous fat and epidermis/dermis, respectively. For V-ECLL, platinum anode and cathode needle electrodes were inserted in a line 2 mm apart using a three-dimensional (3-D) printed jig as guidance (Figure 1A). V-ECLL experiments were conducted at 5 V for 5 minutes (mins). For P-ECLL, platinum needle electrodes for the working ("cathode"), reference, and counter ("anode") electrodes were inserted in a line 2 mm apart using the aforementioned 3-D printed jig (Figure 1B). P-ECLL was conducted at −1, −2, and −3 volts (V) for 5 mins. These are nominal voltage parameters with a potential shift of ±0.5V based on variability in tissue impedance which is influenced by baseline tissue hydration and the chemical product produced.[28] The V-ECLL and P-ECLL treatments were performed twice per condition. Voltage was applied for five minutes based on previous ex vivo ECLL experimental parameters that exhibited the desired adipocyte effect.[25] Charge transfer was recorded throughout the duration of ECLL treatment for offline analysis. These experiments were performed at room temperature.

In Vivo Animal Study Design

Multiple V-ECLL and P-ECLL treatments were performed on the dorsal surface of one female Yorkshire pig (Figure 2A) in order to accommodate serial tissue biopsies immediately after the procedures (day 0) and at days 1, 2, 7, 14 and 28 days. A total of 12 treatment sites were created for each of the following conditions: control, −1.5V P-ECLL, −2.5V P-ECLL, −3.5V P-ECLL, and 5 V V-ECLL for a duration of 5 mins for a total of 60 individual regions. The redundancy for each parameter set was necessary to longitudinally observe changes and allow for two biopsies per condition at each time point (Figure 2B). The two biopsies served to supply enough tissue for histology and fluorescence analysis with morphology and viability.

Animal Care and Anesthesia

The study protocol was performed in accordance with Institutional Animal Care and Use Committee of the University of California, Irvine (IACUC # AUP-17–164). Prior to anesthesia, the Yorkshire pig was sedated with intramuscular injections of telazole (10–11 mg/kg) and xylazine (4–5 mg/kg). Intramuscular enrofloxacin (7.5 mg/kg) was provided for antibiotic prophylaxis. The pig was then intubated and maintained on a ventilator with continuous isoflurane gas (1–3%) administration during ECLL treatment. Lactated Ringer's solution, a standard electrolytic solution composed of sodium chloride (6g/L), sodium lactate (3.1g/L), potassium chloride (0.3g/L), and calcium chloride (0.2g/L),[29] was administered intravenously (4 ml/kg/hr) or subcutaneously (bolus, 25–50 ml) when hydration was required as indicated by skin elasticity and tachycardia. Following experimental procedures, the subject was monitored for excessive pain shown by animal distress, bleeding, infection, and side effects. On Day 28, the animal was euthanized with intravenous pentobarbital sodium/phenytoin sodium (0.3 ml/kg).

V-ECLL & P-ECLL Procedure

Prior to ECLL treatment, depilation was performed by firstly using an electric shaver followed by a single blade razor with shaving cream for a close shave. The treatment grid shown in Figure 2A was drawn on the dorsal surface of the pig using a skin marker. For each given treatment site, 1 ml normal saline was injected in subcutaneous fat and 0.5 ml normal

saline was injected in the epidermis/dermis to provide tissue tumescence in the designated area of ECLL needle insertion. Subsequently, two or three 0.3 mm platinum needles (Grass Technologies, West Warwick RI) were inserted 1 cm into the tumescent tissue for V-ECLL and P-ECLL treatments, respectively. Three needles were inserted into saline-injected normal tissue as well but remained electrically disconnected to create control sites. Using a DC power supply, V-ECLL treatments were conducted at 5V for 5 mins at each assigned site. P-ECLL treatments were conducted using a potentiostat (CH Instruments, Model 650) with an applied potential of −1.5V, −2.5V, and −3.5V over 5 mins according to the treatment grid (Figure 2A). The applied potentials in vivo were greater than that of the ex vivo to compensate for the greater volume of adipose tissue in vivo and to ensure adequate current flow into the system. All potentiostat-based treatments were conducted as bulk electrolysis at a fixed voltage. Temperature elevations with ECT are modest. Previous work measured temperature changes using an infrared focal plane array and thermocouples and was on the order of 1°C at most at the dosimetry setting used.[16,24,25] Following ECLL, the area surrounding the electrode insertion sites of each individual treatment site were tattooed with black ink to provide registry points for each treatment site. Serial 10 mm punch biopsies for each day were taken and hemisected (Figure 2B) to prepare samples for biologic fluorescence assays and histology. Biopsy sites were then sutured closed with 2.0 Vicryl suture (Ethicon Inc., Bridgewater, NJ) and dressed with non-adherent Telfa pads (Covidien, Minneapolis, MN), Tegaderm transparent film (Covidien, Minneapolis, MN), and Ioban drapes (3M, St. Paul, MN). Dressings were removed and replaced at each experimental time point thereafter.

Fluorescence Tissue Staining and Confocal Microscopy

V-ECLL and P-ECLL treated biopsy halves were designated for two fluorescence assays targeting lipid morphology and cell viability. Tissues soaked in 1 N hydrochloric acid (HCl) (Thermo Fisher SA48–1, Waltham, MA) and 1 N sodium hydroxide (NaOH) (Thermo Fisher SS266–1, Waltham, MA) for two hours served as positive controls for the assay to validate the functionality of the staining methods and to maintain the consistency an exceptionally difficult microscopy procedure across image captures. Before and after staining, all tissues were washed three times with HBSS for 10–15 minutes with gentle agitation. Tissues allocated to assess lipid morphology were stained with 800 uL of BODIPY 558/568 C12 (10 ug/ml) and Hoeschst 33342 (2.5 ug/ml) (Invitrogen, Carlsbad, CA), and placed in a 37°C incubator for 45 minutes. BODIPY, a lipophilic dye, was used to stain neutral lipids including adipocytes and lipid droplets, providing morphological information of fat. Hoechst, a cell-permeable dye used to stain cellular DNA regardless of viability status, was utilized to differentiate lipid droplets without nuclei and to identify adipocytes. For the cell live/dead viability assay, designated tissues were stained with 800 uL of Calcein-AM (10 ug/ml), Ethidium Homodimer-1 (EthD-1) (0.75 ug/ml) (Invitrogen E1169, Carlsbad, CA), and Hoechst 33342 (2.5 ug/ml) incubated at 37°C for 45 minutes. Calcein-AM was used to visualize intact and live adipocytes. Calcein-AM is a non-fluorescent cell-permeable dye that is cleaved by intracellular esterases in the cell cytoplasm, enabling green fluorescence. Ethidium homodimer, a non-permeable DNA stain, identifies dead cells that do not have intact cell membranes and fluoresces red. The

subtraction of Hoechst and EthD-1 signals indicates nuclei of live cells. The combination of these dyes, thus, provides positive and negative indicators of cell viability.

An inverted confocal laser scanning microscope (ZEISS LSM 780, Oberkochen, Germany) was used to acquire representative z-stacks with a 10x air objective and tiled images of cross-sectioned biopsy samples following staining. Cellular viability fluorescence utilized an excitation at center wavelength of 488 nm, 405 nm, and 514 nm for Calcein, Hoechst, and EthD-1, respectively. Corresponding fluorescence emission was collected from 490–588 nm for Calcein, 415–484 nm Hoechst, and 589–709 nm for EthD-1. Adipocyte morphology fluorescence was conducted at excitation wavelengths of 561 nm for Bodipy and 405 nm for Hoechst. Corresponding emission fluorescence was collected from 568–672 nm for Bodipy and 415–484 nm for Hoechst.

Histology

Tissues were placed in 10% buffered formalin and processed according to standard protocol before paraffin embedding.[30] Several 8 μm thickness sections surrounding the needle insertion site were placed on glass slides and stained with H&E according to standard protocol.[31] Images of the stained slides were taken at 10x magnification using a light microscope.

Quantitative Analysis of Histology, Morphology, and Live/Dead Viability Assays

BODIPY (lipids), Calcein (live cells), EthD-1 (dead cells), and Hoechst (DNA) stained tissues were analyzed to quantify particle number and area (size) for the respective assays. Individual particles were identified from the unique fluorescent signal and quantified using open-source FIJI software (ImageJ, Bethesda, Maryland). First, a maximum intensity projection was performed on each color channel of the fluorescent images. The images were then denoised using a standard FIJI speckle denoising filter. Subsequently, intensity thresholding created a binary mask where white particles indicated fluorescent signals above a certain user-defined threshold. A binary watershed segmentation algorithm implemented on the binary mask aided in segmenting individual particles that may have combined during the intensity thresholding process. Finally, FIJI's particle analysis algorithm determined the number and size of fluorescent particles. To quantify histological images acquired with light microscopy, adipocyte count and area was calculated using FIJI software. Images were thresholded by intensity to create a binary mask and then underwent binary watershed segmentation. Then the FIJI particle analysis algorithm calculated adipocyte number and area.

Results

Ex vivo Charge Transfer Data

Current and charge transfer as a function of time were compared across dosimetry parameters (Figure 3). Each respective ECLL system measured and recorded current passing through the electrochemical system comprised of platinum needles, saline tumescence and ex vivo porcine tissue. Current was integrated to obtain charge (coulombs) and was plotted as a running sum. Tissue effect is proportional to the generation of acid or base formation

in the tissue which in turn is dependent on the amount of charge transferred.[32,33] It can be seen that P-ECLL dosimetry parameters, namely −2V and −3V P-ECLL, had higher current draw compared to 5V V-ECLL and −1V P-ECLL (Figure 3A). Interestingly, 5V V-ECLL treatments drew more current than −1V P-ECLL treatments, suggesting a potential threshold of P-ECLL dosimetry that fully takes advantage of the feedback control characteristics of a potentiostat. Dosimetry parameters of −2V and −3V P-ECLL exhibited linear and exponential temporal draw, respectively, with eventual leveling off compared to a reduction seen in 5V V-ECLL and −1V P-ECLL. Correspondingly, total charge transfer increased from −1V to −3V P-ECLL and between −1V P-ECLL and 5V V-ECLL, which mirrors in vivo microscopic findings (Figure 3B). Charge transfer rate can be seen by the varying slopes among dosimetry parameters and was highest with −3V P-ECLL and lowest with −1V P-ECLL and 5V V-ECLL. Furthermore, inconsistencies in the charge transfer rate of −2V P-ECLL can be attributed to the formation of gas bubbles that would effectively increase the local bulk resistance of the ECLL treated volume. As the production of bubbles begins to overfill the capacity of the electrochemical treatment volume, they burst, lower the effective bulk tissue resistance, and in turn increase the reaction rate until steady state equilibrium is achieved.

Morphologic Fluorescence

Confocal microscopic tiles of the morphology assay depict red BODIPY signal and blue Hoechst signal (Figure 4), resolving individual adipocyte structure or extracellular lipid droplets, as well as bulk lipid morphology. In all four ECLL experimental conditions, there is loss of viable adipose structure in the treated areas (Figure 4A–P, U–JJ). The diffuse distribution of adipocytes in the normal architecture of untreated adipose tissue is appreciated at the uncharged needle insertion sites (Figure 4Q–T, KK–NN). At the anode, quantitative morphological data shows that compared to the day 0 control, the −3.5V P-ECLL and 5V V-ECLL sites exhibit an increase in small BODIPY stained particles at day 0 (Figure 5A). At subsequent time points, these sites demonstrate a decrease in the number BODIPY stained particles across all particle sizes. Similarly at the cathode, these same trends occur at the −2.5V P-ECLL, −3.5V P-ECLL and 5V V-ECLL sites (Figure 5B). The initial increase in small BODIPY stained particles at day 0 is suggestive of an increase in lipid droplets due to adipocyte lysis. The decrease in larger BODIPY stained particles provides additional evidence of adipocyte lysis while the decrease in the frequency of small BODIPY stained particles at subsequent time points is indicative of lipid droplet absorption by the body. An initial decrease in the area of Hoechst particles from day 0 to 2 for all treatments, aside from that of 5V V-ECLL at the anode, is suggestive of adipocyte death (Figure 5). The subsequent increase in the area of Hoechst particles after day 2 amongst these treatments is likely due to infiltration of polymorphonuclear leukocytes and fibroblasts, as seen with histology described below.

Cellular Viability

Confocal fluorescent images of the cellular viability assay were acquired longitudinally over the 28-day period of the study (Figure 6). On day 0, the appearance of Calcein signal as well as EthD-1 signal indicated the presence of both live and dead cell populations for all dosimetry parameters. From day 0 to day 1 at the anode, there was a decrease

in the Calcein signal at the −2.5V P-ECLL, −3.5V P-ECLL, and 5V V-ECLL treatments suggesting an acute reduction of live cells (Figure 7A). This was also observed at the cathode for −1.5V P-ECLL, −2.5V P-ECLL, −3.5V P-ECLL, and 5V V-ECLL (Figure 7B). The acute inflammatory response seen in light microscopy here is evidenced by the rising Calcein signal observed thru day 14 (Figure 8). This is consistent with the increase in Hoescht signal seen at similar time points (Figure 5). In the untreated control, green Calcein fluorescence in the adipocyte cytoplasm can be observed as the outline of lobular intact adipocytes, indicating live cells with intact cellular membranes at all four timepoints (Figure 6Q–T, KK–NN). There are some subtle differences across dosimetry but the −2.5V P-ECLL, −3.5V P-ECLL, and 5V V-ECLL treatments produced a similar degree of adipocyte death.

Histology

Histology of untreated tissue showed round adipocytes, with eccentric nuclei that are well-organized into lobules. As expected, changes in fat tissue distribution with loss of cell structural regularity and alteration of nuclei were appreciated at “anode” and “cathode” sites following V-ECLL and P-ECLL (Figure 8). On days 14 and 28, recruitment of inflammatory cells, fibroblasts, and collagen deposition were obviously observed in H&E-stained light microscopy images that were consistent with reported results of other minimally and non-invasive adipocyte lysis medical devices (Figure 8),[7,8,34,35] and likely accounted for the positive pinpoint Calcein signal of infiltrative live cells seen in confocal studies (Figure 7). At higher magnification (not shown), the inflammatory reaction was noted on day 7 initially starting at the periphery of the treated sites, and subsequently moved inward to the treated sites. It is very clear that less of an effect is observed in −1.5V P-ECLL treated tissue compared to other dosimetry parameters (Figure 8). Quantitative data from light microscopy images shows a reduction in adipocyte area and frequency over time in the −2.5V P-ECLL, −3.5V P-ECLL, and 5V V-ECLL treatments at the anode compared to control (Figure 9A). At the cathode, a similar decrease is also observed for 1.5V P-ECLL, −2.5V P-ECLL, −3.5V P-ECLL, and 5V V-ECLL treatments (Figure 9B). However, less differences are observed between −2.5V P-ECLL, −3.5V P-ECLL and 5V V-ECLL. This suggests these parameters provide a degree of similarity in treatment which is consistent with that of the morphology and cellular live/dead viability assays (Figure 7).

Discussion

Our group’s preliminary studies have shown that V-ECLL may serve as a low-cost minimally invasive method of lysing adipocytes for medical or cosmetic purposes.[24,25,32,33] However, open-loop V-ECLL has limitations as the current spikes, plateaus, and then decays within the first 30 seconds of treatment, indicating a short time frame during which most charge transfer occurs. Therefore, V-ECLL in its current embodiment is limited in delivering charge and subsequently less efficient at producing sufficient acid and base to induce adipocyte lysis, despite continued voltage application. In this study, we aimed to address these limitations by introducing a potentiostat-based closed-loop, feedback-controlled circuit capable of sensing changes in current flux and adjusting the flow to maintain a constant applied voltage. Our results using morphologic biological fluorescence, cellular live/dead

viability assay, and H&E histology demonstrated similar adipocyte lysis and fat necrosis effects of low voltage P-ECLL compared to higher voltage V-ECLL.

Collectively, all treatment groups demonstrated correlation between lipid droplet formation, adipocyte lysis, denuclearization, and inflammatory response by day 28 consistent with previous reports (Figure 4, 6, 8).[36,37] Previous studies utilized a negative control treatment where similar electrodes were inserted and ECLL treatment was not performed. Histological images from these studies have shown a lack of damage to adipose tissues.[32] This is reflected in the microscopy and histology images of the control tissue over the course of healing (Figure 8). The area of BODIPY and Calcein fluorescent signal loss in 5V V-ECLL was comparable to that of the −2.5V P-ECLL and −3.5V P-ECLL treatments. These findings correlated well with quantitative data from histology, which demonstrated similar lipolytic effects between these three experimental parameters. Ultimately, our findings suggest that low voltage closed-loop, feedback-controlled P-ECLL is as effective as higher voltage open-loop V-ECLL. Understanding the structural components of each system helps explain this phenomenon.

The open-loop V-ECLL circuit is subject to decreasing current draw over time likely due to the consumption of water by electrolysis adjacent to the electrodes. In contrast to the two electrode V-ECLL system, P-ECLL utilizes a three-pronged electrode approach with a closed-loop feedback-controlled circuit to dynamically adjust current flow and maintain a constant potential, effectively creating a reagent diffusion limited system. Feedback-controlled P-ECLL would allow users to obtain a desired ECLL-induced lipolytic effect in a controlled, reproducible manner. The ability to adjust current, and subsequent acid or base production, is critical to achieve varying levels of lipolysis across heterogeneous treatment sites.

Fresh adipose tissue ideally must be sectioned to produce a sharp cleavage plane for imaging, this is a fundamental technical limitation, because fresh fat is viscoelastic and jelly-like. The uneven cleavage planes result in irregular surface contours which means that tissue may not be within the focal plane of the microscope at a specified depth. This occurs with all fresh (non-frozen) tissue imaging. “Dark” areas seen in BODIPY images are frequently regions that lie out of the imaging plane of the confocal system. Compensating for this effect, we acquired z-stack fluorescent volumetric data capable of imaging into the sample plane eliminating any non-planar sample cross-sectioning artifact. Regardless, the changes in tissue morphology demonstrate adipocyte lysis and cell death and are consistent with each fluorescent technique and histology. In addition to the oxygen-evolving reaction that occurs at the platinum anode, the high concentration of NaCl within the tissue likely results in some oxidation of chloride to chlorine. Notably, in aqueous solution Cl_2 rapidly disproportionates to hypo- and hydrochloric acids (HClO and HCl), which also lower the pH.[38] Although the thermodynamic potential for chloride oxidation is more than 0.5V higher than the $4e^-$ oxidation potential of water,[39] the kinetics of Cl_2 evolution are typically more rapid than the oxygen-evolving reaction,[40] so the extent of hypochlorite production is unknown. Of note, bulk morphological depressions on the pig dorsum were not visualized up to day 28 in this study, despite microscopic findings of fat necrosis. The clinical effect of ECLL in adipose tissue is generally observed after 3-months as triglycerides take time to be absorbed

by the body. At day 28, these lipid deposits remain in the tissue, preventing the clinical observation of fat loss.[41] Due to the costly and labor-intensive nature of survival porcine studies, this study was limited to one subject. Although the sample size does not allow for statistical significance, trends can be suggested. Future studies are needed to investigate ECLL-induced adipose changes at longer time points and increase statistical power.

Additionally, P-ECLL systems are technically more complex, requiring a more intricate feedback circuit with three needles compared to a V-ECLL system that requires only two needles. The addition of a reference needle provides the means to probe the system dynamically for changes in current flow and facilitates the monitoring and control of the ECLL process. This is more difficult to accomplish with V-ECLL where both short and open circuits may be harder to detect. A third needle also makes needle insertion into thick porcine epidermis and dermis more challenging for the P-ECLL compared to the two V-ECLL treatment needles. However, this could be overcome with a mechanism to constrain the needles to one another, such as a custom-fitted jig, and is more a design and manufacturer issue than an intrinsic limitation of the technology. Accordingly, needles should be sharpened to medical specifications to facilitate easier insertion.

Conclusion

Both V-ECLL and P-ECLL have shown their fat necrosis effects in this exploratory in vivo longitudinal animal model. Fat treated with V-ECLL and P-ECLL undergoes destruction through adipocyte membrane lysis, triglyceride saponification, and denuclearization, which triggers an innate immune response and fat necrosis. However, we have shown that differences in treatment areas vary between the two approaches yielding that higher voltage V-ECLL produces a comparable lipolytic effect as lower voltage P-ECLL. Our findings suggest that a closed-loop feedback-controlled P-ECLL system may offer enhanced control of current transmission and thus spatially selective tissue injury compared to its open-loop V-ECLL counterpart, which enables ECLL's potential use for precision adipose tissue reduction in discrete regions. Both techniques are focused therapies, in contrast to existing technologies which achieve fat reduction with low spatial resolution. Investigations are underway to optimize electrode placement for use in clinical settings.

Acknowledgements:

This research was supported by the following funding sources: George E. Hewitt Foundation, Irvine Head and Neck Research Foundation, Laser Microbeam and Medical Program (LAMMP) Grant funded by the National Institutes of Health/National Institute of Biomedical Imaging and Bioengineering (NIH/NIBIB) (P41-EB015890), the Chao Cancer Center Grant funded by the National Cancer Institute (NIH/NCI) (2P30CA062203-19), University of California Irvine Beal Applied Innovation Proof of Product Grant (POP 443803-19954), the John Stauffer Charitable Trust, and the Leading Foreign Research Institute Recruitment Program through the National Research Foundation of Korea (NRF) funded by the Ministry of Science and ICT (MSIT) (NRF-2018K1A4A3A02060572).

Appendix A

In a simple DC experiment, two electrodes are connected to a power supply which applies a voltage difference, *e.g.,* 5V, between them.[28] The "electrochemical potential" of those voltages however, relative to an external reference-the normal hydrogen electrode (NHE) typically-is unknown. In contrast, the non-linear circuitry of a three-electrode potentiostat

allows the application of a precise electrochemical potential at a single electrode. Please note that potential and potential difference are two different entities.

At pH 7, the reduction of water to H_2 and OH^- ($2\ H_2O + 2e^- \rightleftharpoons H_2 + 2\ OH^-$) occurs at −0.41V vs. NHE (NHE is the electrochemical potential for the reaction: $2H^+ + 2e^- \rightleftharpoons H_2$ at pH 0), while the oxidation of water to O_2 and H^+ ($2\ H_2O \rightleftharpoons O_2 + 4H^+ + 4e^-$) occurs at +0.82V vs. NHE. The gap between these two reactions is 1.23V. In principle, using a potentiostat we can select an electrochemical potential at the working electrode that can selectively reduce water by applying any potential of −0.41V or less (at pH 7).[42] In practice, that reaction is typically slow at the thermodynamic potential and requires an "overpotential"; in this application, potentials of −1.5V or lower are typically required to generate OH^- at an appreciable rate; moreover, as the reaction occurs the pH rises, shifting the thermodynamic potential for hydrogen evolution more negative by 59mV per pH-unit rise.

It is important to note that a variety of electrochemical reactions can take place outside of this −0.41 to +0.82 (vs. NHE) potential window: the reduction of dioxygen to superoxide, for example, on the negative side, or the oxidation of chloride to chlorine, water to hydrogen peroxide, or water to the hydroxyl radical on the positive side. Thus when applying a DC voltage of 5V, we cannot control the possible chemical reactions *that might occur* because we do not know what the electrochemical potentials are at the cathode and anode—only that they are 5V apart. In principle a DC voltage difference of 1.23V would be sufficient to electrolyze water, but that would require that the electrochemical potential at the anode were poised exactly at 0.82 and the cathode were poised exactly at −0.41V. The DC power supply does not allow us to control those electrochemical potentials; and once the electrolysis begins, the electrochemical potentials for hydrogen and oxygen evolution shift in response to pH changes, so the electrolysis reaction would quickly cease. That is why we practically have to apply much greater voltages than 1.23V using a DC power supply. A 5V gap is so large that the cathode potential surely sits negative of the threshold value for hydrogen evolution, while the anode potential sits well positive of the threshold value for oxygen evolution. But these (unknown) electrochemical potentials are so extreme as to cause *other chemical reactions in addition to simple water electrolysis*. In contrast, the potentiostat treatment allows us to selectively apply an electrochemical potential at a single electrode, thus allowing us to drive a specific chemical reaction within the tissue in a controlled manner.

References

1. Body Fat Reduction Market Share Analysis 2019–2025 Statistics Report. Available at: https://www.gminsights.com/industry-analysis/body-fat-reduction-market?utm_source=prnewswire.com&utm_medium=referral&utm_campaign=Paid_prnewswire. Accessed October 11, 2019.
2. Global Medical Aesthetics Market Report 2019–2025. Available at: https://www.prnewswire.com/news-releases/global-medical-aesthetics-market-report-2019-2025-300910273.html. Accessed September 12, 2019.
3. Rao RB, Ely SF, Hoffman RS. Deaths related to liposuction. N Engl J Med. 1999;340(19):1471–1475. doi:10.1056/NEJM199905133401904 [PubMed: 10320385]

4. Franco W, Kothare A, Ronan SJ, Grekin RC, McCalmont TH. Hyperthermic injury to adipocyte cells by selective heating of subcutaneous fat with a novel radiofrequency device: Feasibility studies. Lasers Surg Med. 2010;42(5):361–370. doi:10.1002/lsm.20925 [PubMed: 20583242]
5. Avci P, Nyame TT, Gupta GK, Sadasivam M, Hamblin MR. Low-Level Laser Therapy for Fat Layer Reduction: A Comprehensive Review. Lasers Surg Med. 2013;45(6):349–357. doi:10.1002/lsm.22153 [PubMed: 23749426]
6. Saedi N, Kaminer M. New waves for fat reduction: high-intensity focused ultrasound. Semin Cutan Med Surg. 2013;32(1):26–30. [PubMed: 24049926]
7. Ingargiola MJ, Motakef S, Chung MT, Vasconez HC, Sasaki GH. Cryolipolysis for Fat Reduction and Body Contouring: Safety and Efficacy of Current Treatment Paradigms. Plast Reconstr Surg. 2015;135(6):1581–1590. doi:10.1097/PRS.0000000000001236 [PubMed: 26017594]
8. Ascher B, Fellmann J, Monheit G. ATX-101 (deoxycholic acid injection) for reduction of submental fat. Expert Rev Clin Pharmacol. 2016;9(9):1131–1143. doi:10.1080/17512433.2016.1215911 [PubMed: 27457304]
9. Badran KW, Manuel CT, Loy AC, Conderman C, Yau YY, Lin J, Tjoa T, Su E, et al. Long-term in vivo electromechanical reshaping for auricular reconstruction in the New Zealand white rabbit model. Laryngoscope. 2015;125(9):2058–2066. doi:10.1002/lary.25237 [PubMed: 25779479]
10. Yau AYY, Manuel C, Hussain SF, Protsenko DE, Wong BJF. In vivo needle-based electromechanical reshaping of pinnae new Zealand white rabbit model. JAMA Facial Plast Surg. 2014;16(4):245–252. doi:10.1001/jamafacial.2014.85 [PubMed: 24854476]
11. Hussain S, Manuel CT, Protsenko DE, Wong BJF. Electromechanical reshaping of ex vivo porcine trachea. Laryngoscope. 2015;125(7):1628–1632. doi:10.1002/lary.25189 [PubMed: 25692713]
12. Tracy LE, Wong BJ. The Effect of pH on Rabbit Septal Cartilage Shape Change: Exploring the Mechanism of Electromechanical Tissue Reshaping. Eplasty. 2014;14:e23. [PubMed: 25165492]
13. Kim S, Manuel CT, Wong BJF, Chung PS, Mo JH. Handheld-Level Electromechanical Cartilage Reshaping Device. Facial Plast Surg. 2015;31(3):295–300. doi:10.1055/s-0035-1555623 [PubMed: 26126226]
14. Manuel CT, Tjoa T, Nguyen T, Su E, Wong BJF. Optimal Electromechanical Reshaping of the Auricular Ear and Long-term Outcomes in an In Vivo Rabbit Model. JAMA Facial Plast Surg. 2016;18(4):277–284. doi:10.1001/jamafacial.2016.0166 [PubMed: 27101542]
15. Hunter BM, Kallick J, Kissel J, Herzig M, Manuel C, Protsenko D, Wong BJF, Hill MG. Controlled-Potential Electromechanical Reshaping of Cartilage. Angew Chem Int Ed Engl. 2016;55(18):5497–5500. doi:10.1002/anie.201600856 [PubMed: 27059655]
16. Protsenko DE, Ho K, Wong BJF. Stress relaxation in porcine septal cartilage during electromechanical reshaping: Mechanical and electrical responses. Ann Biomed Eng. 2006;34(3):455–464. doi:10.1007/s10439-005-9051-y [PubMed: 16450186]
17. Manuel CT, Foulad A, Protsenko DE, Sepehr A, Wong BJF. Needle electrode-based electromechanical reshaping of cartilage. Ann Biomed Eng. 2010;38(11):3389–3397. doi:10.1007/s10439-010-0088-1 [PubMed: 20614240]
18. Protsenko DE, Ho K, Wong BJF. Survival of chondrocytes in rabbit septal cartilage after electromechanical reshaping. Ann Biomed Eng. 2011;39(1):66–74. doi:10.1007/s10439-010-0139-7 [PubMed: 20842431]
19. Lim A, Protsenko DE, Wong BJF. Changes in the tangent modulus of rabbit septal and auricular cartilage following electromechanical reshaping. J Biomech Eng. 2011;133(9):094502. doi:10.1115/1.4004916 [PubMed: 22010748]
20. Kuan EC, Hamamoto AA, Manuel CT, Protsenko DE, Wong BJF. In-depth analysis of pH-dependent mechanisms of electromechanical reshaping of rabbit nasal septal cartilage. Laryngoscope. 2014;124(10):E405–E410. doi:10.1002/lary.24696 [PubMed: 24687330]
21. Badran K, Manuel C, Waki C, Protsenko D, Wong BJF. Ex vivo electromechanical reshaping of costal cartilage in the New Zealand white rabbit model. Laryngoscope. 2013;123(5):1143–1148. doi:10.1002/lary.23730 [PubMed: 23553270]
22. Manuel CT, Foulad A, Protsenko DE, Hamamoto A, Wong BJF. Electromechanical reshaping of costal cartilage grafts: a new surgical treatment modality. Laryngoscope. 2011;121(9):1839–1842. doi:10.1002/lary.21892 [PubMed: 22024834]

23. Oliaei S, Manuel C, Karam B, Hussain SF, Hamamoto Ashley, Protsenko SE, Wong BJF. In vivo electromechanical reshaping of ear cartilage in a rabbit model: A minimally invasive approach for otoplasty. JAMA Facial Plast Surg. 2013;15(1):34–38. doi:10.1001/2013.jamafacial.2 [PubMed: 23117484]
24. Pham TT, Hong EM, Moy WJ, Zhao J, Hu AC, Barnes CH, Borden PA, et al. The biophysical effects of localized electrochemical therapy on porcine skin. J Dermatol Sci. 2020;97(3):179–186. doi:10.1016/j.jdermsci.2020.01.006 [PubMed: 32169274]
25. Pham TT, Stokolosa AM, Borden PA, Hansen KD, Hong EM, Krasieva TB, Sivoraphonh RH, et al. Electrochemical degradation and saponification of porcine adipose tissue. Sci Rep. 2020;10(1):20745. Published 2020 Nov 27. doi:10.1038/s41598-020-76678-y [PubMed: 33247200]
26. Pease WS, Grove SL. Electrical safety in electrodiagnostic medicine. PM R. 2013;5(5 Suppl):S8–S13. doi:10.1016/j.pmrj.2013.03.019 [PubMed: 23523704]
27. Goolsby AD, Sawyer DT. Versatile Solid-State Potentiostat and Amperostat. https://pubs.acs.org/sharingguidelines. Accessed September 12, 2019.
28. Bard BJ, Faulkner LR. Chapter 15: Electrochemical Instrumentation. In: Bard BJ, Faulkner LR. Electrochemical Methods: Fundamentals and Applications. 2nd ed. Wiley; 2002: 1364–1365
29. Smiley KE, Debas HT, deVries CR, Price RR. Global Surgery. In: Brunicardi F, Andersen DK, Billiar TR, Dunn DL, Kao LS, Hunter JG, Matthews JB, Pollock RE. eds. Schwartz's Principles of Surgery, 11e. McGraw-Hill; Accessed March 08, 2021. https://accesssurgery.mhmedical.com/content.aspx?bookid=2576&sectionid=216218501
30. Layton C, Bancroft JD, Suvarna SK. 4 - Fixation of tissues. In: Suvarna SK, Layton C, Bancroft JD, eds. Bancroft's Theory and Practice of Histological Techniques (Eighth Edition). Elsevier; 2019:40–63.
31. Fischer AH, Jacobson KA, Rose J, Zeller R. Hematoxylin and eosin staining of tissue and cell sections. CSH Protoc. 2008;2008:pdb.prot4986. Published 2008 May 1. doi:10.1101/pdb.prot4986 [PubMed: 21356829]
32. Hutchison DM, Hakimi AA, Hong EM, et al. Electrochemolipolysis of Human Adipose Tissue. Facial Plast Surg Aesthetic Med. 2020;22(2):86–92. doi:10.1089/fpsam.2019.29011.hut
33. Hu AC, Hong EM, Toubat O, et al. Multiphoton Microscopy of Collagen Structure in Ex Vivo Human Skin Following Electrochemical Therapy. Lasers Surg Med. 2020;52(3):196–206. doi:10.1002/lsm.23094 [PubMed: 31124173]
34. Meyer PF, Silva RMV, Oliveira G, Tavares MA, Medeiros ML, Andrada CP, Neto LG. Effects of Cryolipolysis on Abdominal Adiposity. Case Rep Dermatol Med. 2016;2016:1–7. doi:10.1155/2016/6052194
35. Walker PS, Lee DR, Toth BA, Bowen B. Histological Analysis of the Effect of ATX-101 (Deoxycholic Acid Injection) on Subcutaneous Fat. Dermatologic Surg. 2019;101:1. doi:10.1097/dss.0000000000001851
36. Alizadeh Z, Halabchi F, Mazaheri R, Abolhasani M, Tabesh M. Review of the mechanisms and effects of noninvasive body contouring devices on cellulite and subcutaneous fat. Int J Endocrinol Metab. 2016. doi:10.5812/ijem.36727
37. Rzany B, Griffiths T, Walker P, Lippert S, McDiarmid J, Havlickova B. Reduction of unwanted submental fat with ATX-101 (deoxycholic acid), an adipocytolytic injectable treatment: Results from a phase III, randomized, placebo-controlled study. Br J Dermatol. 2014. doi:10.1111/bjd.12695
38. Wang TX, Margerum DW. Kinetics of Reversible Chlorine Hydrolysis: Temperature Dependence and General Acid/Base-Assisted Mechanisms. Inorg. Chem. 1994: 33, 1050. DOI: 10.1021/ic00084a014
39. Wood PM. The potential diagram for oxygen at pH 7. Biochem J. 1988;253(1):287–289. doi:10.1042/bj2530287 [PubMed: 2844170]
40. Chen Z, Concepcion JJ, Song N, Meyer TJ. Chloride-assisted catalytic water oxidation. Chem Commun (Camb). 2014;50(59):8053–8056. doi:10.1039/c4cc04071f [PubMed: 24924315]
41. Wollina U, Goldman A. ATX-101 for reduction of submental fat. Expert Opin Pharmacother. 2015;16(5):755–762. doi:10.1517/14656566.2015.1019465 [PubMed: 25724831]

42. Eliaz N, Gileadi E. Chapter 3: Fundamental Measurements in Electrochemisty. In: Eliaz N, Gileadi E. Physical electrochemistry: Fundamentals, techniques, and applications. 6th ed. Wiley; 2019;doi:10.1002/anie.201104618

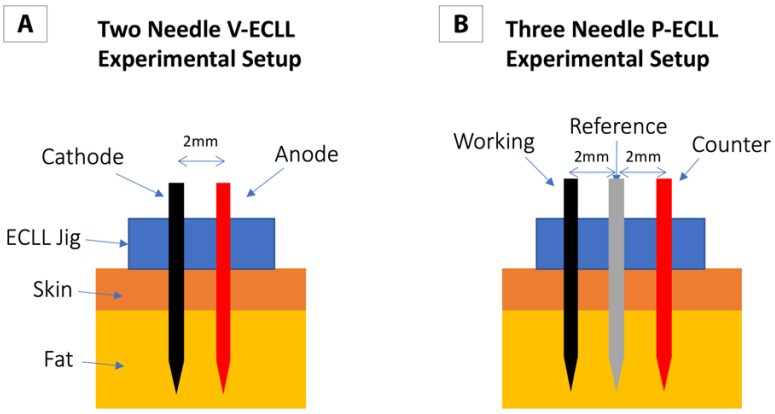

Figure 1:

(A) Two needle V-ECLL ex vivo experimental setup (B) Three needle P-ECLL ex vivo experimental setup wherein the working electrodes were held at potentials that reduced water to H_2 and OH^-, corresponding to the "cathode" reaction in V-ECLL; the counter electrode therefore affected water oxidation and generation of H^+, similar to the "anode" reaction in V-ECLL.

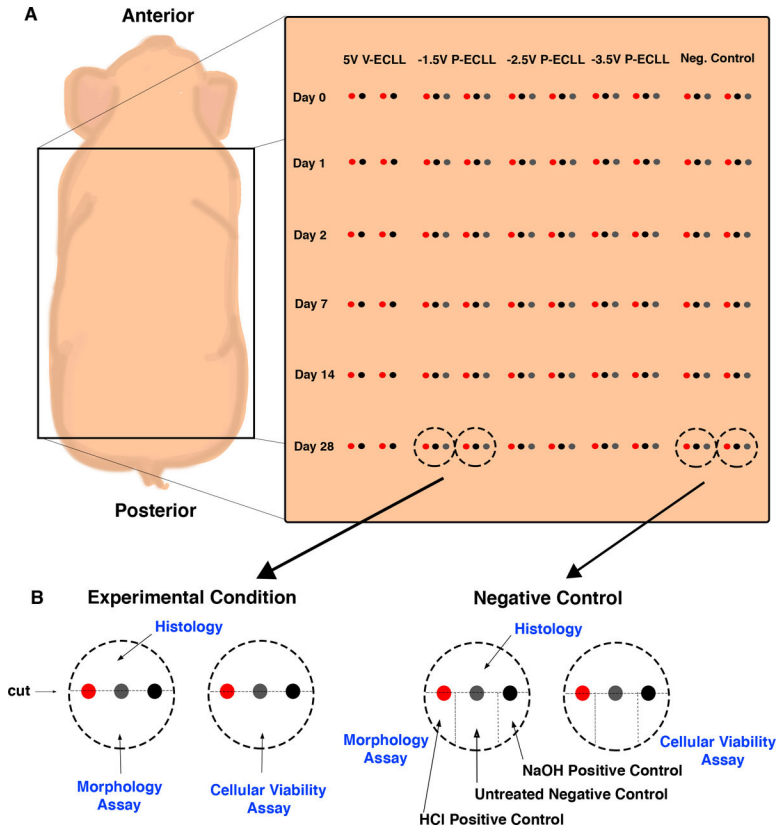

Figure 2:

(A) Schematic diagram of treatment grid applied to the dorsal surface of a female Yorkshire pig. Red circles indicate “anode” electrodes, gray circles indicate reference electrodes, and black circles indicate “cathode” electrodes. The dashed circle indicates the 10mm punch biopsy site taken at ECLL treated sites and untreated control sites. Two biopsies per condition were taken at each time point. (B) Detailed schematic breakdown of the punch biopsy segments utilized for the morphology assay, cellular live/dead viability assay, and histology. Dotted lines indicate cuts that were made to segment the circular biopsy. For the fluorescence assays, tissues segments were used for the untreated and positive controls [hydrochloric acid (HCl) and sodium hydroxide (NaOH)].

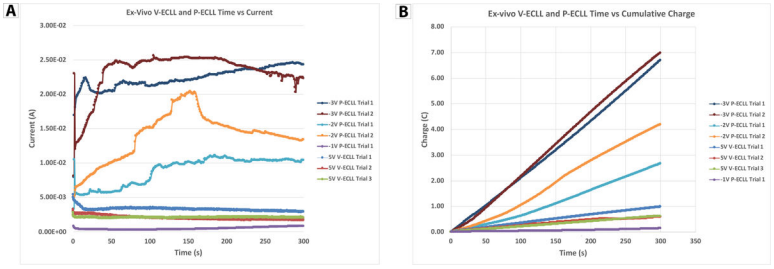

Figure 3:

(A) Ex vivo V-ECLL and P-ECLL current versus time curves for all dosimetry parameters. (B) Ex vivo V-ECLL and P-ECLL cumulative charge versus time curves for all dosimetry parameters.

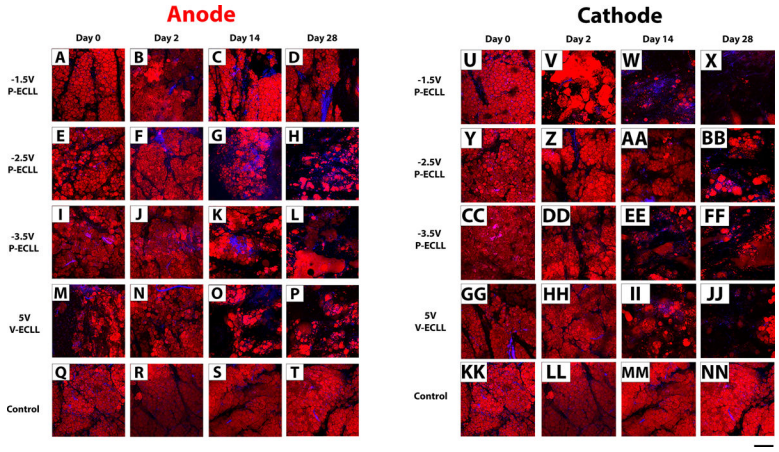

Figure 4:

Morphology assay of V-ECLL and P-ECLL treated porcine fat at varying dosimetry followed longitudinally over 28 days at the anode and cathode. Ten mm punch biopsy half sections were stained with neutral lipid stain BODIPY 558/568 (shown in red) and DNA stain Hoechst 33342 (shown in blue). Samples from (A-D, U-X) −1.5V P-ECLL, (E-H, Y-BB) −2.5V P-ECLL, (I-L, CC-FF) −3.5V P-ECLL, and (M-P, GG-JJ) 5V V-ECLL treated samples for 5 minutes shown after 2, 7, 14 and 28 days post treatment. Control samples at each timepoint are shown in Q-T, KK-NN.

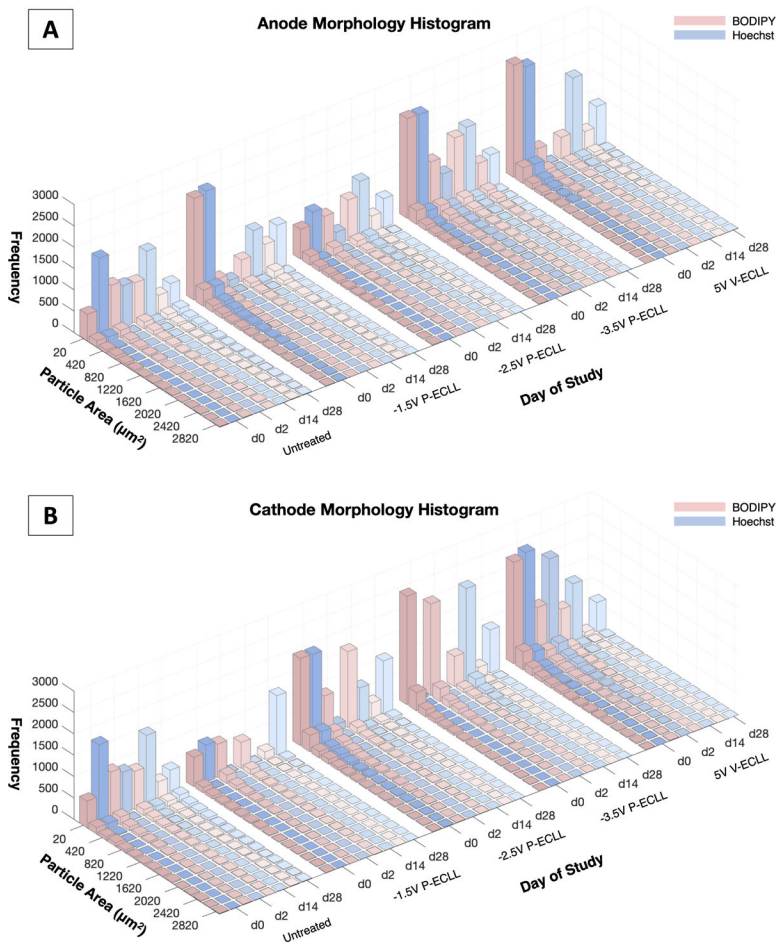

Figure 5:

BODIPY 558/568 and Hoechst 33342 particle area count of V-ECLL and P-ECLL treated regions at the (A) anode and (B) cathode sites longitudinally over 28 days.

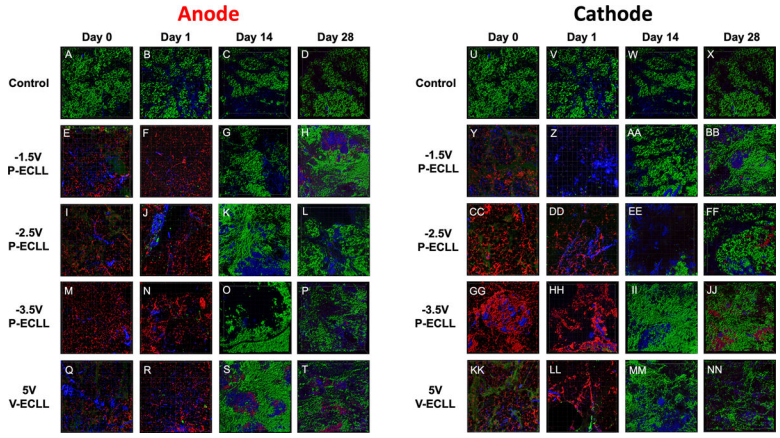

Figure 6:

Live/dead viability assay of V-ECLL and P-ECLL treated porcine fat at varying dosimetry followed longitudinally over 28 days. Ten mm punch biopsy half sections were stained with fluorescent “live” Calcein-AM cytoplastic stain (green), “dead” Ethidium Homodimer (EthD-1) stain (red), and “all nucleic acid” Hoechst nuclear stain (blue). Samples from (A-D, U-X) −1.5 V P-ECLL, (E-H, Y-BB) −2.5 V P-ECLL, (I-L, CC-FF) −3.5 V P-ECLL, (M-P, GG-JJ) 5 V V-ECLL treated for 5 minutes shown after 1, 7, 14 and 28 days post treatment. Control samples at each time point are shown in Q-T and KK-NN.

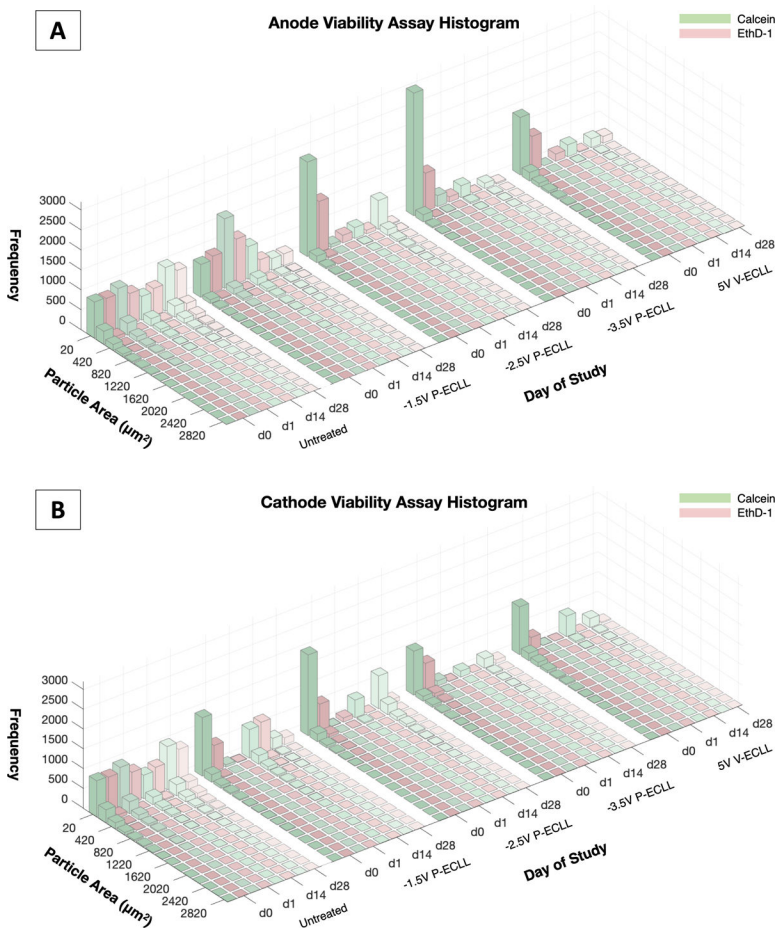

Figure 7:

Calcein-AM and Ethidium Homodimer (EthD-1) particle area count of V-ECLL and P-ECLL treated regions at the (A) anode and (B) cathode sites longitudinally over 28 days.

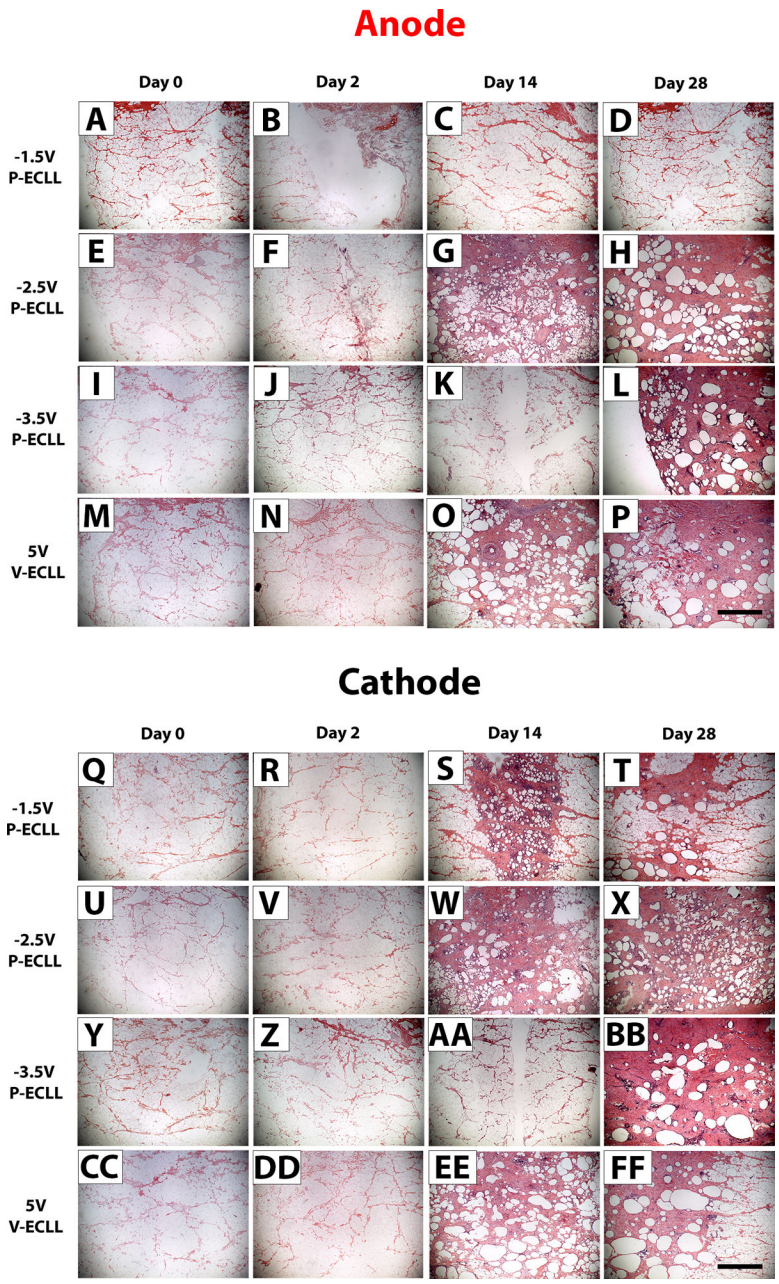

Figure 8:

Histology of V-ECLL and P-ECLL treated regions followed longitudinally over 28 days. Histology at the anode (A-T) and cathode (U-NN) with varying treatment voltages.

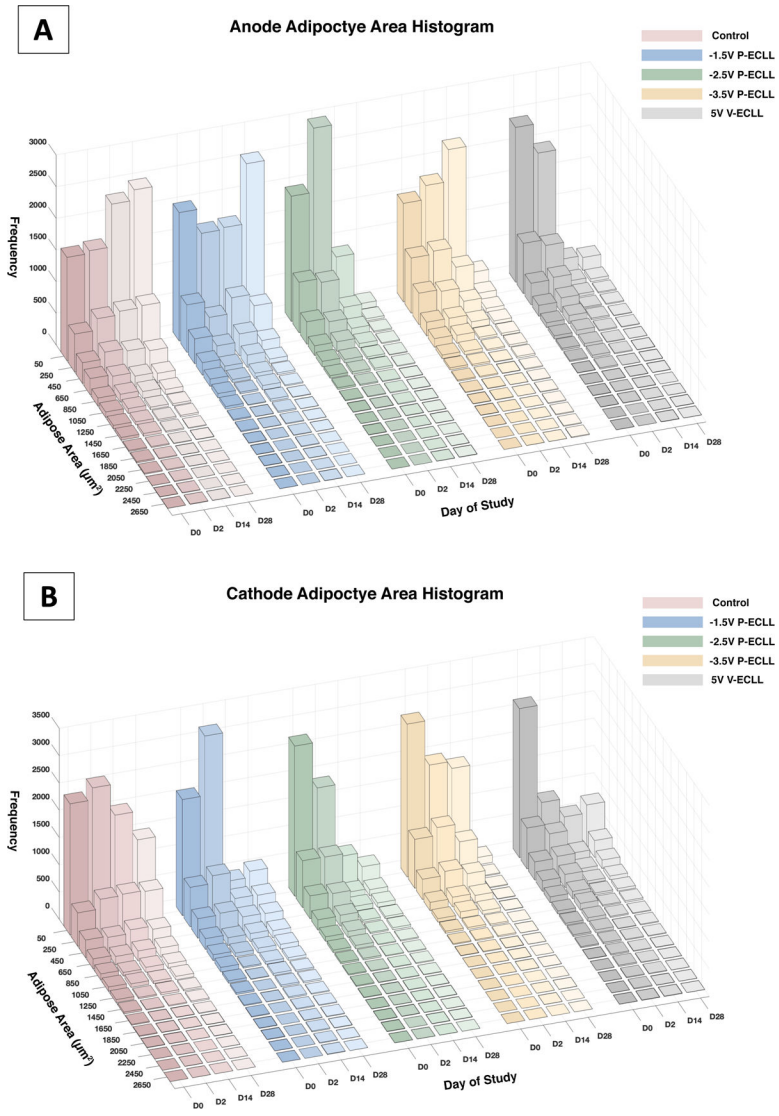

Figure 9:

Histological adipocyte area count of V-ECLL and P-ECLL treated regions at the (A) anode and (B) cathode sites longitudinally over 28 days.